Metasurface-Tunable Lasing Polarizations in Microcavity

ZHIYI YUAN,[1][¥] SHIH-HSIU HUANG,[2][¥] ZHEN QIAO,[1] PIN CHIEH WU,[2][★] YU-CHENG CHEN[1][★]

[1] *School of Electrical and Electronic Engineering, Nanyang Technological University, 50 Nanyang Avenue, 639798, Singapore*

[2] *Department of Photonics, National Cheng Kung University, Tainan 70101, Taiwan*

[¥] *These authors contributed equally*

[★]*pcwu@gs.ncku.edu.tw;* [★]*yucchen@ntu.edu.sg*

Abstract: Manipulating polarization states of microlasers is essentially important in many emerging optical and biological applications. Strategies have been focused on using external optical elements or surface nanostructure to control the polarization state of laser emission. Here we introduce a fundamentally new strategy for manipulation of laser polarization based on metasurface through round trips of photons confined inside an active optical cavity. The role of intracavity metasurface and light-meta-atoms interactions were investigated under a stimulated emission process in a microcavity. Taking advantage of strong optical feedback produced by the Fabry-Perot optofluidic microcavity, light-meta-atoms interactions will be enlarged, resulting in polarized lasing emission with high purity and controllability. Depending on the metasurface structural orientation, the polarization state of a lasing emission can be actively modulated as linearly polarized or elliptically polarized with different degrees of circular polarization at source within microcavity. This study provides a new insight into fundamental laser physics, opening new possibilities by bridging metasurface into microlasers.

1. Introduction

Microlasers have attracted tremendous attention owing to their remarkable tunability and their promising potential for miniaturized light sources.[1-4] Advances in microlasers have demonstrated the possibility to manipulate lasing properties in various aspects, including lasing direction, emission wavelengths, chirality, and polarizations.[5-8] Among which, the ability to manipulate the polarization state of laser is fundamental yet crucial in many applications such as polarization-sensitive imaging, circular dichroism spectroscopy, *etc*.[9-11] In principle, stimulated emission photons travel back and forth within the optical cavity to form standing waves before reaching laser oscillation. Owing to the coherence nature of stimulated emission, excited photons only excite new photons with the identical polarization state.[12] The polarization state of laser output is therefore solely determined by the initial pump laser polarization. As the scale of laser becomes smaller down to micro-and nanoscale nowadays, tuning the laser polarization turns out to be a critical challenge. Over the years, scientists have been investigating methods for manipulating lasing polarizations on the micro to nanoscale optics. Conventional approaches take advantage of external optical elements such as linear polarizer, quarter-wave plate (QWP), and half-wave plate (HWP) to control the polarization state of laser emission.[13] Designing the optical properties of micro/nanostructures or

materials is another widely accepted concept to manipulate lasing polarizations nowadays. For instance, controlling the lasing polarizations through the external or surface structure of a microlaser device.[14, 15] However, manipulating lasing polarization through round trips of photons inside an optical microcavity remains elusive.

Metasurfaces, consisting of subwavelength metallic or dielectric nanoscatterers (meta-atoms), have been proposed as a new paradigm to control and manipulate light-matter interactions.[16] Such nanoscatterers strongly interact and re-emit photons with defined polarization, phase, and momentum, thus allowing efficient light manipulation. Metasurface has demonstrated its ability on wavefront engineering in both free space light beams and laser sources as an external optical component.[17-19] To date, nearly all the metasurface generate its function based on "one-time interaction" with light, either optical reflection/transmission[20] or photon emissions from luminescent materials.[21] Very less attention has been paid to multiple light-metasurface interactions. Embedding metasurface in an optical microcavity not only enhances the interactions between meta-atoms and light but adds another degree of freedom to control the cavity resonance. For instance, ultrastrong coupling and ultrathin cavity have been accomplished through metasurface with passive optical resonators.[22, 23] High purity orbital angular momentum beams were also realized through an intra-macrocavity metasurface.[18] To the best of our knowledge, the role of intracavity metasurface has never been investigated in any active optical resonators, especially microlasers.

For the first time, the role of intracavity metasurface was investigated experimentally and theoretically in an active microlaser resonator. We surprisingly discovered that the physics behind light-metasurface interaction is very much different when meta-atoms are located at the surface or embedded in a microcavity. Taking advantage of strong optical feedback generated by Fabry-Perot (FP) microcavity, light-meta-atoms interactions can be remarkably extracted and amplified. Our findings demonstrate that the polarization state of a lasing emission can be actively modulated and controlled at source with a metasurface-embedded microcavity. Figure 1 illustrates the concept of metasurface structure confined in an optofluidic laser microcavity, in which Aluminum nanoantennas were directly fabricated on the surface of a distributed Bragg reflector (DBR) substrate. In this configuration, the polarization state of light is modified once interacted with the metasurface-structured DBR (meta-DBR) until the polarization state is expected to reach stable condition and coherence. The cavity mode can be decomposed into a pair of orthogonal polarization eigenmodes: the <X> and <Y>.[24] As the structural orientation angle θ (the angle between the long-axis of meta-atom and the linear polarization direction of pump laser) changes, the amplitude ratio of <X> and <Y> changes, as well as the phase difference between <X> and <Y>, leading to the modulation of polarization state of laser emission. Depending on the cavity/structural orientation, the generated laser beam can be linearly polarized, or elliptically polarized with either low or high degree of circular polarization (DOCP) at source. The orientation angle-dependent path of lasing polarization state on the Poincaré sphere were provided to verify the versatility of metasurface-embedded microcavity for polarization engineering.
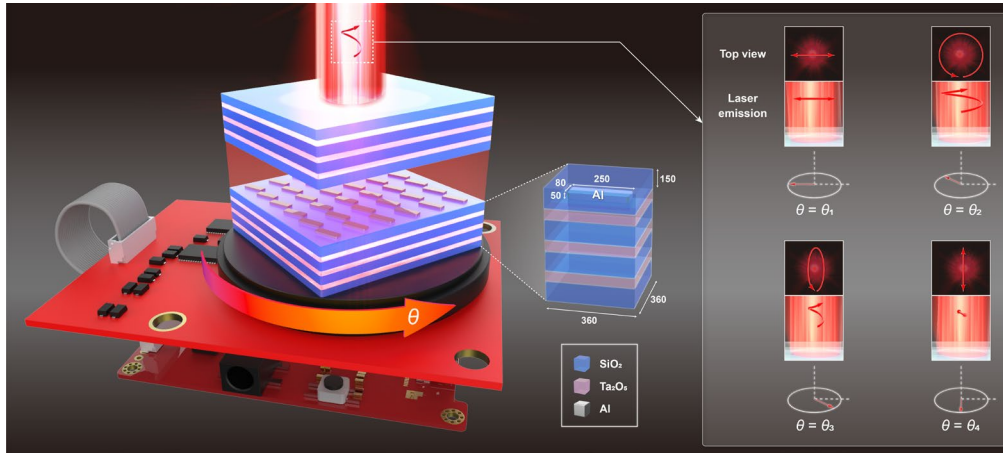
Fig. 1. Schematic of metasurface structures embedded inside of an optofluidic microlaser cavity. The polarization state of the laser beam can be dynamically modulated at source via the metasurface orientation. In this work, linearly polarized or elliptically polarized laser with certain DOCP are realized. The dimensions of the metasurface unit element are shown on the inset of the left panel (unit: nm). The right panel schematically illustrates the metasurface-orientation-dependent lasing polarization.

2. Results

2.1 Design and concept of metasurface-embedded microcavity

As shown in the inset of Fig. 1, Al metasurface elements were embedded in a 150-nm-thick SiO$_2$ layer to ensure that the plasmonic resonant wavelength of nanoantennas would not be affected by its surrounding aqueous spectrally shift after introducing the fluorescent dye into the microcavity (Fig. 1). It is worth mentioning that the utilization of subwavelength nanostructures should not significantly influence the beam quality after introducing the metasurfaces into the microcavity, which shows the benefits of this design. In addition, the SiO$_2$ layer can also assist in avoiding the oxidation issue of Al. Please notice that during the meta-atom optimization, the optical phase delay in the SiO$_2$ cladding layer had been considered. To generate different polarization states via superposition effect, an anisotropic meta-atom is designed to support two orthogonal plasmonic eigen-states (which can be decomposed into <X> and <Y>) under a linearly polarized illumination. By controlling the amplitude ratio and phase difference between two plasmonic eigen-states which can be practically realized through tuning the structural orientation with respect to the <X> and <Y> directions, versatile polarizations including linearly polarized and elliptically polarized with low/high degree of circular polarization lasing emission can be obtained (refer to Fig. 1). In this study, this is achieved through rotating the metasurface-embedded microcavity (see left panel of Fig. 1).

To design metasurface-embedded microcavity accordingly, we begin from "one-time light-meta-atom interaction". The physical concept of the proposed metasurface element for polarization engineering is shown schematically in Fig. 2a. The inset shows the scanning electron microscope (SEM) images of fabricated Al metasurface (see Fig. S1 for details of the nanofabrication flow for the metasurface). To simplify, the optical response of the metasurface is theoretically investigated with a plane wave under normal illumination. For a linearly *x*-polarized incidence, the reflected beam only contains either *x*-polarized or *y*-polarized component if the structural orientation angle $\theta = m\pi/2$, where m is an integer. This is because only one single plasmonic eigen-mode can be accessed when incident polarization is along the symmetric axes of the Al nanoantenna. Figs. 2b and 2c respectively show the numerically simulated co-polarized and cross-polarized reflection spectra of the optimized Al nanoantenna.

When tuning the structural orientation, the amplitude of both co-polarized and cross-polarized components keep almost unchanged at the wavelength of pump laser (530 nm). Since slight intensity variation can be significantly amplified after introducing the microcavity,[25] such a nearly constant intensity response allows us to flexibly modulate the polarization state through metasurface-induced resonances without considering the influence from pumping source. In contrast, the intensity of reflected beams is dramatically modulated at the wavelength of lasing output (~565 nm). The phase response also plays a vital role for polarization manipulation. Fig. 2d shows the simulated phase difference between two orthogonal components as a function of wavelength and structural orientation angle. Similarly, a significant modulation of the phase response is achieved at the photon emission wavelength by rotating the Al nanoantenna, revealing the ability of the metasurface for polarization control for lasing source. To further explore the generated polarization state at the wavelength of ~565 nm where the fluorescence emission occurs, the Stokes parameters, which can represent the states of polarization on the Poincaré sphere, are introduced (see Fig. 2e). The Stokes parameters can be calculated as (also refer to supplementary note 1):

$$S_1 = \left| E_y \right|^2 - \left| E_x \right|^2 \tag{1}$$

$$S_2 = 2Re\left[E_y E_x^* \right] \tag{2}$$

$$S_3 = -2Im\left[E_y E_x^* \right] \tag{3}$$

The normalized stokes parameters (s_1, s_2, s_3):

$$s_i = \frac{S_i}{\sqrt{\sum_{i=1}^{3} S_i^2}} \tag{4}$$

As expected, the reflected beam possesses a linear polarization ($s_1 \approx$ -1, $s_2 \approx s_3 \approx 0$) when the structural orientation angle $\theta = 0$, $\pi/2$, and π. It is worth noticing that the polarization state of reflected light must be always parallel to the incident polarization when that is along the symmetric axes of the Al nanoantenna. As discussed, the amplitude ratio and phase difference can be actively modulated by tuning the structural orientation angle θ. Thus, we expect to obtain different polarization states when tuning the structural orientation. As the structural angle θ increases from 0° to 45° , the polarization state of reflected beam is converted from a linear x-polarization to a nearly left-handed circular polarization (LCP) through a transition of a left-handed elliptical polarization (LEP). When the θ is further increased from 45° to 135° , the polarization state is switched from LCP to a nearly right-handed circular polarization (RCP) via transitions from a LEP to a linear y-polarization and eventually to a right-handed elliptical polarization (REP).
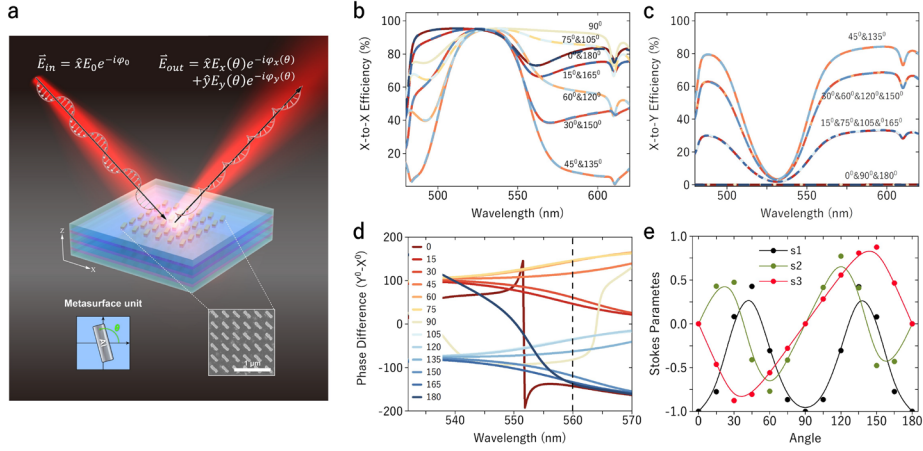
Fig. 2. (a) Schematic illustration of the metasurface elements on a DBR substrate (meta-DBR). The bottom-right inset shows SEM image of fabricated metasurface. Both the amplitude and phase of the reflected light along *x*-direction and *y*-direction are modulated under an *x*-polarized illumination. The simulated reflectance spectra of co-polarization and cross-polarization components with various structural angles θ are shown in **(b)** and **(c)**, respectively. **(d)** Simulated phase difference between co-polarized and cross-polarized reflection as a function of structural angle θ. **(e)** Calculated Stokes parameters carried out from **(b)** and **(c)**.

2.2 Characterization of elliptically polarized lasing output with high degree of circular polarization

The experimental results (see Fig. S2 for the optical setup for sample characterization) highly match with the numerical prediction, which further confirms that the designed Al nanoantennas are capable of converting the incoming light with a fixed polarization into various polarization states with structural orientation. To clearly verify the optical response of the fabricated metasurface, the measured Stokes parameters at other wavelengths are provided in Fig. S3. The polarization state remains almost unchanged at a wavelength of 530 nm, indicating that both the amplitude and phase of the pumping light cannot be modulated by the metasurface for any *θ*. This is highly consistent with the numerical simulations shown in Figs. 2b-2d: only the dye fluorescence emission can be adjusted by the meta-atoms in our metasurface-embedded microcavity laser.

Moving forward, we used this meta-DBR (bottom mirror) and another normal DBR (top mirror) to form a FP microcavity. The optical properties of microcavity can be modified by the embedded metasurface, resulting in different lasing phenomena. The experimental setup is provided in Fig. S4, in which laser gain material Rhodamine 6G (R6G) is sandwiched in the FP cavity. The excitation and collection were implemented through the same objective and optical pathway. R6G was selected as the gain medium due to its high quantum yield and suitable spontaneous emission band (Fig. S5). Fig. 3a presents the lasing spectra of R6G within metasurface-embedded microcavity under various pump energy densities, where the cavity length is 28 µm. Fig. 3b shows spectrally integrated laser output as a function of pump energy, where a threshold of 72 µJ mm^{-2} was observed. Above this pump energy, the linewidth of emission spectra decreases rapidly, indicating the lasing threshold behavior (refer to Fig. 3a for the lasing spectra). To verify the polarization states of laser emission, we insert a QWP and a linear polarizer into the home-made optical system (see Figs. 3c and 3d). When the fast axis of QWP was aligned with 45º to the *x* axis, the Jones matrix of QWP can be expressed as:

$$M_{QWP} = \frac{1}{\sqrt{2}}\begin{pmatrix} 1 & i \\ i & 1 \end{pmatrix} \tag{5}$$

In addition, the Jones matrix of circularly polarized light is described by:

$$E = \frac{1}{\sqrt{2}}\begin{pmatrix} 1 \\ \pm i \end{pmatrix} \tag{6}$$

where the positive and negative represent RCP and LCP light, respectively. If LCP light passes through the QWP, outgoing light polarization becomes perpendicular with the *x* axis (90°):

$$E_{QWP} = \frac{1}{2}\begin{pmatrix} 1 & i \\ i & 1 \end{pmatrix}\begin{pmatrix} 1 \\ i \end{pmatrix} = \begin{pmatrix} 0 \\ i \end{pmatrix} \tag{7}$$

In contrast, the outgoing light polarization becomes parallel with the *x* axis (0°) if RCP light passes through the QWP:

$$E_{QWP} = \frac{1}{2}\begin{pmatrix} 1 & i \\ i & 1 \end{pmatrix}\begin{pmatrix} 1 \\ -i \end{pmatrix} = \begin{pmatrix} 1 \\ 0 \end{pmatrix} \tag{8}$$

As a result, the light polarization can be decomposed and analyzed through the combination of QWP and linear polarizer. As can be seen in Fig. 3e, when the structural orientation angle θ is 45° , the LCP laser output is much larger than the RCP laser output. Next, we measured the laser emission intensity as a function of polarizer angle with and without the QWP (Fig. 3g). After passing through the QWP, the laser output was converted to a linear polarized light (90°), which is consistent with the above discussions. The degree of circular polarization ($DOCP = \frac{I_{RCP} - I_{LCP}}{I_{RCP} + I_{LCP}}$) equals to −0.7. In contrast, the laser output exhibits more likely the RCP characteristics when the structural orientation angle θ is 135° (refer to Fig. 3f). Please notice that the intensity presented here is spectrally integrated from 560 nm to 570 nm, thus, a linear-polarization-like intensity profile in the orange curve does not support the generation of a linearly-polarized laser emission at 135°. Fig. 3h shows the $DOCP$ of laser output is around 0.7. These results clarify that the metasurface plays a role to determine the polarization state of the laser output. To further verify this concept, we subsequently analyzed the polarization state of lasing emissions from a conventional FP microcavity (in the absence of metasurface), as shown in Figs. S6a and S6b. Theoretically, the polarization state of the laser output is identical with the pump laser, which is experimentally observed in our result (see Fig. S6c). This is because excited state photons not only excite new photons with the identical polarization state, but fluorophores dipole with an orientation close to the pumping polarization angle will also be preferentially excited (known as fluorescence polarization).[8] This small fluorescence polarization preference will be amplified within the microcavity during laser oscillation process, leading to the identical laser output polarization. Albeit the coherent metasurface has been reported for incoherent emission engineering,[26, 27] we emphasize that the metasurface's capability for polarization control of incoherent emission here is weak even multiple light-meta-atom interactions occur. To verify this point, we investigate the polarization state of fluorescence emission under the same configuration (below the lasing threshold). Fig. S7a shows that fluorescence generated from a conventional microcavity is almost unpolarized, which is consistent with previous reports.[8] When the metasurface is involved with a structural orientation angle θ of 45° or 135° , the fluorescence emissions exhibit similar elliptical polarization properties but much lower DOCP than the laser output (Figs. S7b-c). In short, these results indicate that the optical resonance in metasurface and stimulated emission process play critical roles in the light-metasurface interactions.

Our findings above clearly show that the laser emission generated from metasurface-embedded microcavity can achieve high degree of circular polarization. In the laser oscillation, the light intensity in a cavity suddenly increases with time, starting from a small initial intensity I_0. As such, the light intensity at time t can be written as:

$$I(t) = I_0 \exp[(\gamma_0 - \alpha)ct] \tag{9}$$

$$\alpha = \frac{1}{2L}\ln(\frac{1}{R_1 R_2}) + \alpha_0 \tag{10}$$

where γ_0 is the gain coefficient, α_0 is the absorption of gain material, c is speed of light in vacuum, L is cavity length, R_1 and R_2 are the reflectivity of two mirrors, and α is the total cavity loss. Here, we define a parameter, normalized inversion ratio r, which is the ratio between the laser gain and total cavity loss:

$$r = \frac{\gamma_0}{\alpha} = \frac{2L\gamma_0}{\ln(\frac{1}{R_1 R_2}) + 2\alpha_0 L} \tag{11}$$

Therefore, Eqn. (9) can be expressed as:

$$I(t) = I_0 \exp[\frac{r-1}{\tau_c}t] \tag{12}$$

where τ_c is the cavity lifetime $\tau_c = \dfrac{2nL}{c[\alpha_0 + \ln(\frac{1}{R_1 R_2})]}$. The buildup time is given by:

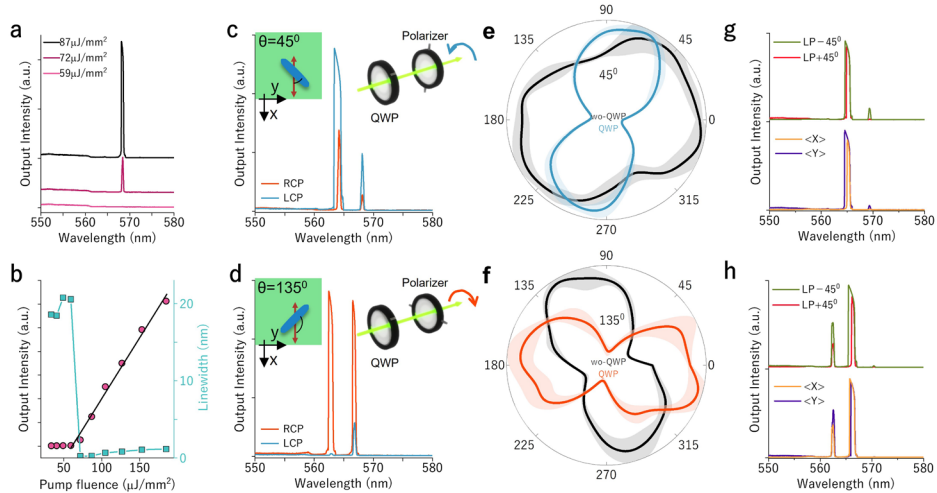$$T_b \approx \frac{\tau_c}{r-1}\ln\left(\frac{I_s}{I_0}\right) \tag{13}$$

Fig. 3. (a) Lasing spectra of 1 mM R6G within the metasurface-embedded microcavity, the curves have been vertically shifted for clarity. **(b)** Spectrally integrated laser output and linewidth under various pump energy densities. **(c-d)** LCP

and RCP lasing spectra generated from metasurface-embedded cavity with an orientation angle of **(c)** 45° and **(d)** 135°. Top-right inset shows the schematic diagram of QWP and linear polarizer. Under the same angle of QWP (45°), polarization state of laser is LCP or RCP when passing through different angles of polarizer (0° or 90°). **(e)** Spectrally integrated (560-570nm) laser emission intensity generated from metasurface-embedded cavity under an orientation of 45°, as a function of the polarization angle with (blue line) and without (black line) QWP. **(f)** Spectrally integrated (560-570nm) laser emission intensity generated from metasurface-embedded cavity under an orientation of 135°, as a function of the polarization angle with (orange line) and without (black line) the QWP. **(g-h)** x-polarized, y-polarized, LP-45°, and LP-135° polarized lasing spectra generated from metasurface-embedded cavity under an orientation of **(g)** 45° and **(h)** 135°. LP: linear polarization.

2.3 Effect of cavity length on lasing output polarization

Noted that the laser oscillation buildup time is highly related to cavity lifetime as well as cavity length. To investigate the influence of cavity length on lasing polarization, laser emission generated from different cavity lengths were collected. Fig. 4a plots the lasing spectra from the metasurface-embedded microcavity with a 33-µm-thick cavity. The cavity length was confirmed by measuring the free-spectral-range (FSR = $\lambda^2/2md$, where m is the refractive index and d is the cavity length), where a FSR of 3.6 nm was obtained. Same as the previous case, the laser emission exhibits high degree of circular polarization where LCP output generated from the 45° -oriented metasurface and RCP output generated from the 135° -oriented metasurface (Figs. 4b and 4c). Next, we changed the cavity length to 45 µm, where FSR equals to 2.7 nm (Figs. 4d). The same polarization states of laser emission produced by this cavity length (Figs. 4e and 4f), denoting that cavity length does not alter the polarization states of laser output. Light interacts with metasurface within microcavity could result in different polarization states in each round trip. However, this counterintuitively result indicates that light polarization states are expected to be stable in the laser oscillation process.

To interpret the cavity length independence, we decompose the cavity into a pair of orthogonal polarization modes <X> and <Y>, which are projected from <L> and <S> that are defined as the eigen-modes along long-axis and short-axis of meta-atom, respectively. At resonance, phase shift resulted from two orthogonal polarization modes (<L> and <S>) round-trip inside the FP cavity should follow:

$$\frac{4\pi mL}{\lambda_l} + \varphi_{m1} + \varphi_{m2} + \varphi_l = 2\pi m_l \tag{14}$$

$$\frac{4\pi mL}{\lambda_s} + \varphi_{m1} + \varphi_{m2} + \varphi_s = 2\pi m_s \tag{15}$$

where L is the thickness of the cavity, m is the refractive index of the gain material. φ_{m1} and φ_{m2} are the extra phase shifts induced by the top DBR and bottom meta-DBR mirrors. φ_l and φ_s are the phase shift induced by the metasurface. In the experiments, <L> and <S> modes are excited at the same wavelength. According to the Eqns. (14) and (15), the phase of <L> or <S> shifts the integer times of 2π. This is due to the self-consistency characteristics of laser. Therefore, the phase difference between two orthogonal polarization modes has been determined once the laser oscillation builds up, resulting in the observation of above cavity-length-independent lasing polarization.
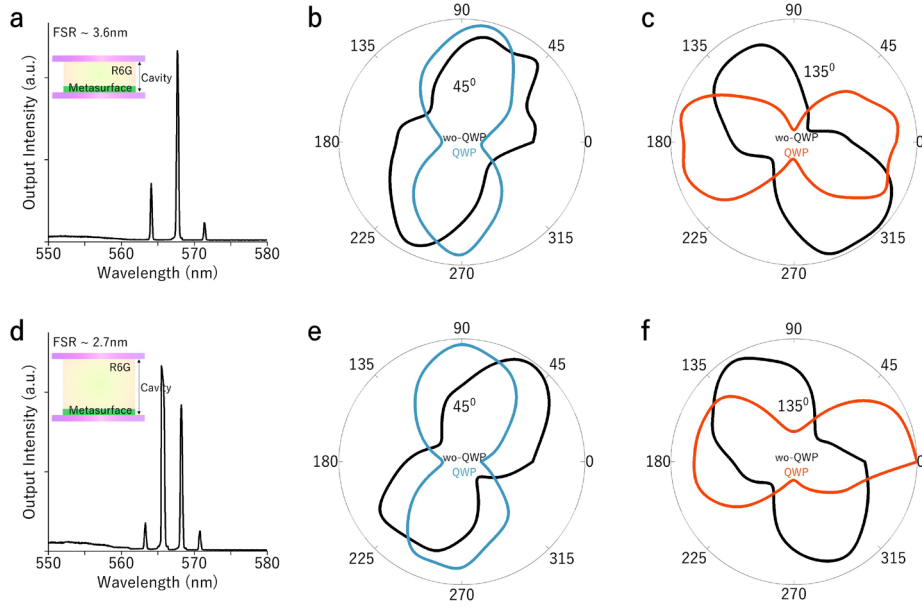
Figure 4. (a) Lasing spectra of 1 mM R6G within the metasurface-embedded microcavity with a cavity length of 33 μm. **(b, c)** Laser emission intensity generated from a 33-μm-thick metasurface-embeddded microcavity with orientation angle of **(b)** 45° and **(c)** 135° as a function of the polarization angle with (color lines) and without (black lines) the QWP. **(d)** Lasing spectra of 1 mM R6G within the metasurface microcavity with cavity length of 45 μm. **(e, f)** Laser emission intensity generated from a 45-μm-thick metasurface-embedded microcavity with orientation angle of **(e)** 45° and **(f)** 135° , as a function of the polarization angle with (color lines) and without (black lines) the QWP. The detected wavelength range for **(b)**, **(c)**, **(e)**, and **(f)** is 560-570 nm. Lasing from 563-573 nm were collected and integrated to plot **(b-c)** and **(e-f)**.

2.4 Effect of output side on lasing output polarization

Since the metasurface is solely present on the surface of one of the mirrors, the lasing polarization possesses a space-asymmetric property. Fig. 5a illustrates the schematic diagram of laser oscillation within metasurface-embedded microcavity, where laser can emit from both top mirror (normal DBR) and bottom mirror (meta-DBR). In a conventional laser oscillation, laser polarization state remains the same inside the cavity due to the coherence nature. Under linear polarization pump, the top laser output possesses the same polarization state as the laser emitting from bottom mirror; under circular polarization pump, the top laser output presents an opposite polarization state compared with the laser emitting from bottom mirror. In contrast, the proposed metasurface-embedded microcavity possess a very different response for light travelling both inside and outside the microcavity with respect to the polarization state (refer to Fig. 5a). For instance, once the forward and backward light travel inside the microcavity has the <X> polarization (depends on the metasurface orientation), while the bottom laser output can possess the <Y> polarization due to the interaction with metasurface. In this assumption, metasurface switches the transmitted light into the opposite points on the Poincaré sphere, and then modifies it back when it was reflected. Same as the conventional FP cavity, the backward laser wave inside the cavity is LCP when the forward laser wave inside the cavity is RCP for the metasurface-embedded microcavity. Our findings in Fig. S3 show the polarization of reflected light does not overlap with the same point of Poincaré sphere (after passing through

the HWP twice). Meta-DBR provides amplitude and phase modulations before the laser builds up. In the steady state, it works as a HWP because of the laser self-consistency characteristics (the laser oscillation self-consistency requires the roundtrip phase difference of oscillation mode to be equal to an integer multiple of 2π).[28]

To verify the above-mentioned theory, experimental studies were systematically carried out. Fig. 5b shows the measured Stokes parameters of top laser output as a function of the structural orientation angle θ. As can be seen, the s_3 reaches the minimum and the maximum at the angle of 45° and 135°, respectively. At the angle of 90°, s_1 equals to -1, which means the polarization state of laser output is same as the pump laser. When the angle is 0°, s_1 is close to 1, which means the polarization state of laser output is perpendicular to the pump laser. These results are completely distinguishable from the observations in the "one-time light-meta-atom interaction" in which the reflected polarized polarization is always parallel to the incident one (see discussions for Figs. 2 and 6). Each point of laser output polarization state can be plotted on the Poincaré sphere as shown in Fig. 5c. It is noteworthy that both the chirality and the orientation of the polarization states vary remarkably as a function of the structural orientation angle θ. The polarization state follows the trajectory on the Poincaré sphere which passes through the equator, highlighting the transition from elliptical to linear polarization. Such strong and exotic angular dependence of polarization state demonstrates the huge potential of polarization control. On the other hand, lasing polarizations and spectrum output from the bottom mirror were also collected and plotted in Fig. S8. For comparison, polarization states as a function of angle are plotted in Figs. 5d and 5e. Interestingly, the polarization states of bottom laser output are located approximately at opposite points ($s_1, s_2, s_3 \rightarrow -s_1, -s_2, -s_3$) on the Poincaré sphere, verifying the assumption in Fig. 5a.
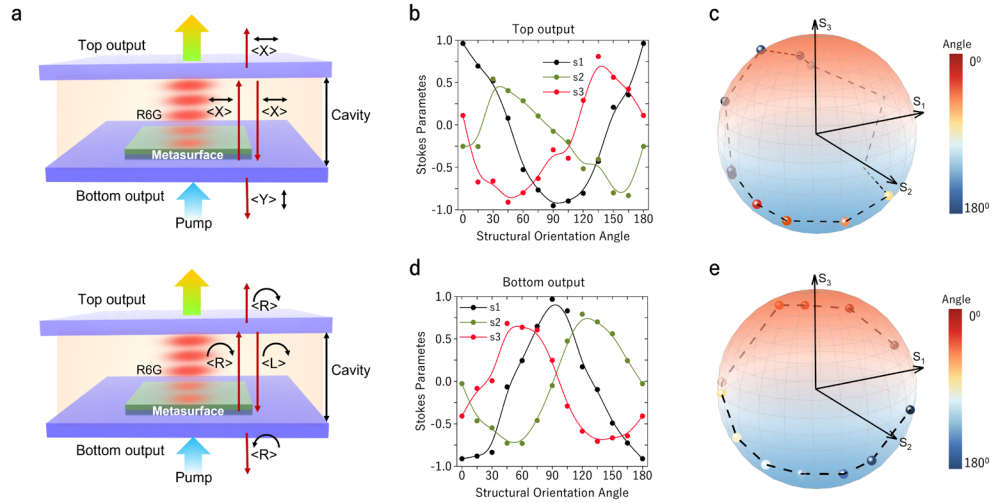

Figure 5. (a) Schematic illustration of laser oscillation within a metasurface-embedded microcavity, where the polarization state of laser was changed after interacting with the meta-DBR. Measured normalized Stokes parameters (S_1, S_2, S_3) of **(b)** top laser output and **(d)** bottom laser output as a function of metasurface angle. Measured normalized Stokes parameters of **(c)** top laser output and **(e)** bottom laser output on the Poincare sphere.

2.4 Principle of metasurface-embedded microlaser

To elucidate the role of metasurface in a microlaser cavity, here we carried out theoretical simulations for better understanding of intracavity light-metasurface interactions. Figure 6a illustrates the entire laser oscillation buildup process in a metasurface-embedded microcavity.

Initially, organic dye molecules are excited to higher energy states by the pump laser. Next, spontaneous emission noise photons (initial intensity I_0) are produced by the excited dye molecules in the cavity. Although spontaneous emission photons show a broadband feature, only the photons which match the cavity mode can be amplified. During the laser buildup process, fluorescence polarization is amplified within the microcavity. At the same time, metasurface modulates the fluorescence emission polarization depending on the amplitude ratio and phase difference between the long-axis <L> and short-axis <S> of meta-atom. Consequently, the light intensity continuously increases due to the stimulated emission and finally reaches a steady-state level (laser gain equals to total cavity losses α) with a defined polarization state. In the steady state, metasurface finally acts as a half-wave plate (see in Fig. 5a) so that the stable standing wave can be supported in the metasurface-embedded microcavity. Since the optical loss is dramatically amplified in the cavity process, the absorption in meta-atom plays a vital role in determining the lasing polarization. To verify this model, the absorption spectrum of the meta-DBR is provided (see Fig. S9). When structural angle is 0°, the high optical absorption in meta-atom along x-direction leads to a lasing beam emission with polarization normal to the meta-atoms (see Fig. 5b). As a result, the amplitude ratio of laser output between <L> and <S> is mainly dependent on the absorption anisotropic of metasurface. The phase difference between <L> and <S> is mainly dependent on the metasurface reflection during the laser buildup process.

According to the above-mentioned laser oscillation principle, an amplitude-based standing wave is anticipated inside the laser cavity instead of a polarization standing wave.[29, 30] To verify this concept, time-dependent field distributions inside the microcavity are provided (see Figs. 6b and S10). Apparently, the polarization states are independent in the z-position, indicating the generation of an amplitude-based standing wave. In addition, we found that the LCP component possesses the highest intensity over the microcavity under structural orientation angle of 45°, while RCP possesses the highest at 135°. These agree well with our experimental observations (see Figs. 3 and 5). The field distribution outside the laser cavity shows similar distributions inside the microcavity (see Fig. S12), showing that the lasing polarization state is closely correlated with the standing wave response. Next, we define rate equations which describe the population dynamics of excited state molecules density and photons density, as described by Eqns. (16) to (19). The photons are emitted into a superposition of the cavity eigen-modes.

$$\frac{dn_l}{dt} = I_p \delta_{abs}(N_0 - n_l - n_s) - \frac{c}{m}\sigma_e q_l n_l + \frac{c}{m}\sigma_a q_l (N_0 - n_l - n_s) - \frac{n_l}{\tau_f} \qquad (16)$$

$$\frac{dq_l}{dt} = \frac{c}{mV}\sigma_e n_l + \frac{c}{m}\sigma_e q_l n_l - \frac{c}{m}\sigma_a q_l (N_0 - n_l - n_s) - \frac{q_l}{\tau_l} \qquad (17)$$

$$\frac{dn_s}{dt} = I_p \delta_{abs}(N_0 - n_l - n_s) - \frac{c}{m}\sigma_e q_s n_s + \frac{c}{m}\sigma_a q_s (N_0 - n_l - n_s) - \frac{n_s}{\tau_f} \qquad (18)$$

$$\frac{dq_s}{dt} = \frac{c}{mV}\sigma_e n_s + \frac{c}{m}\sigma_e q_s n_s - \frac{c}{m}\sigma_a q_s (N_0 - n_l - n_s) - \frac{q_s}{\tau_s} \qquad (19)$$

Assuming that both L- and S-aligned orientations can achieve lasing under the condition of single mode, in the above equations, n_l, n_s, q_l, and q_s respectively represent the densities of dye molecules in the first excited state, and the densities of the photons which have L- and S-polarized orientation. σ_e and σ_a are respectively the emission and absorption cross sections, at the dye lasing wavelength. I_p is the time-dependent pump intensity, and N_0 is the concentration of dye molecules. c and m respectively describe the speed of light in vacuum and refractive index of the solvent. τ_f denote the fluorescence lifetime. V is the mode volume. We assume the pump is a Gaussian temporal profile with $I_p = I_{p0} \times \exp\left(-4ln2[\frac{t-t_0}{\Delta t}]^2\right)$, Δt is the pulse duration (5 ns). τ_l and τ_s denote the photon lifetime of the cavity mode <L> and <S>, where photo lifetime is determined by the reflectivity of mirrors ($\tau_c \approx \frac{2nL}{c(1-R_1 R_2)}$, $\tau_l \approx 0.54$ ps; $\tau_s \approx 0.83$ ps). As can be seen in Fig. S9, the absorption of structural angle 0° (pump light polarization is along to long-axis of meta-atom) is much higher than the absorption of structural angle 90°. As such, the reflectivity of mode <L> is lower than the mode <S>, resulting in shorter photon cavity lifetime. According to the Eqns. (16) to (19), the amplitude of <L> and <S> mode can be obtained. Combining with the phase difference in Fig. 2d, we can theoretically calculate the Stokes parameters of simulated lasing output. Subsequently, the Stokes parameters of lasing output at laboratory coordinate can be transferred through the coordination rotation (supplementary note 2). The simulated results in Figs. 6c and 6d show the similar trend with the experimental results in Fig. 5b, validating the proposed physics model.
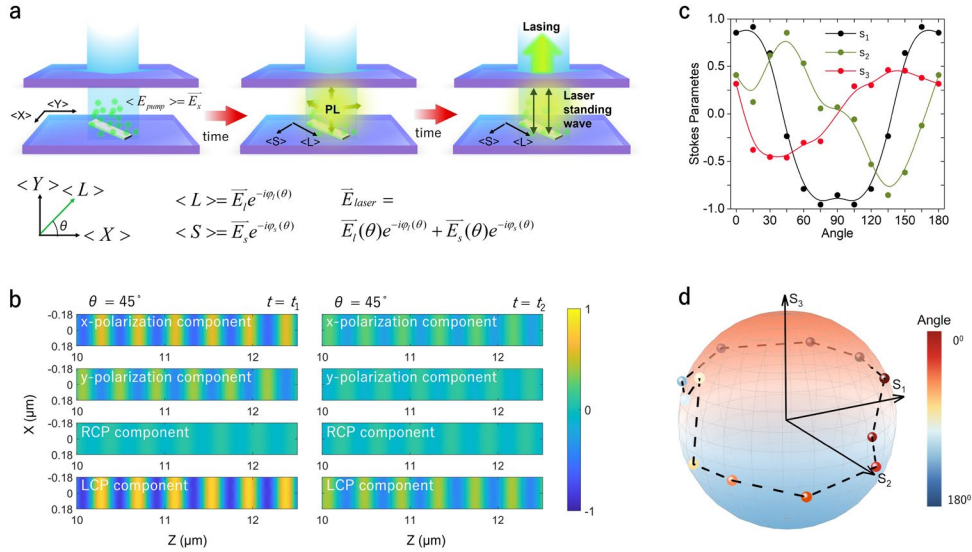

Figure 6. (a) Schematic illustration of laser oscillation buildup process. Fluorophores (in green dots) excited by the pump laser; excited photons reflected back and forth within metasurface-embedded microcavity and stimulate more photons (photoluminescence); lasing with a defined polarization state was achieved after the laser oscillation process. (b) Time-dependent polarization distribution inside the metasurface-integrated microcavity. The structural orientation angle is fixed at 45°. The time difference $\Delta t = t_2 - t_1 = 1.877$ fs, which equals half period of the light propagation inside the cavity (cavity length = 28 μm). For simplicity, only the central region of the microcavity is shown. The metasurface is located at z = 0 μm. Wavelength: 563 nm. Simulated normalized Stokes parameters of laser output **(c)** as a function of metasurface angle and **(d)** on the Poincare sphere.

3. Discussion and Conclusion

In this study, we investigated the fundamental physics of light-meta-atoms interactions under a stimulated emission process. Our findings demonstrate that the polarization state of a lasing output can be actively modulated and controlled at source with a metasurface-embedded microcavity. According to our theory-guided experimental results, the microcavity length does not alter the polarization states of laser output. This counterintuitive result indicates that polarization states of photons inside the metasurface-embedded microcavity are expected to be stable in the laser oscillation process. Based on our analyses and theoretical simulations, the underlying mechanism has been proposed which intracavity metasurface changes the transmitted photons to the opposite points on the Poincaré sphere, and then modifies it back when it was reflected. Simulation results were also carried out and agreed well with the experimental observations. Indeed, the position of metasurface can significantly influence the lasing polarization state (Fig. S11). Precise design of the metasurface and laser cavity must be considered to accommodate different optical applications. The concept of metasurface-embedded microlaser cavity can be extended to control different lasing functions by designing the structures of metasurface, such as chirality and vortex beams. Note that the current laser gain material can be replaced with any aqueous type of gain materials, including quantum dots, fluorescent proteins, biomoeclules, and dyes. To enhance the stability of lasing output, the gain material may be replaced by solid-state materials such as perovskites, quantum dots, or even semiconductor nanocrystals in future. We would like to point out that metallic meta-structures may increase the lasing threshold due to strong optical absorption. However, this could be possibly addressed by replacing the plasmonic meta-atoms with high-index all-dielectric metasurfaces. Thanks to the high flexibility of both the metasurface and wide variety of optofluidic laser gain materials, the operating wavelength can be practically shifted from visible to near infrared regions with desired wavelengths. Lastly, we would like to point out that the current study was demonstrated within a microscale laser cavity; however, we envision intracavity metasurface may be able to function with nanolasers or polariton lasers with a smaller cavity size.

4. Methods

4.1 Optical system setup

For the excitation of the Fabry-Pérot microcavity and the collection of laser emission, an inverted microscopic system (Nikon Ti2) with 20X 0.4 NA objective was used. Optical pumping was achieved by a pulsed ns-laser (EKSPLA NT230) integrated with an optical parametric oscillator (repetition rate: 50 Hz; pulse duration: 5 ns). According to the respective absorption wavelength of fluorophores, the pump laser was tuned to 530 nm for R6G. The beam diameter at the objective focal plane was ~16 μm wide. The collected light was sent into an imaging spectrometer (Andor Kymera 328i).

4.2 Fabry-Pérot microcavity

The Fabry-Pérot microcavity was found by two dielectric mirrors. For one of the dielectric mirrors (distributed Bragg reflectors) which reflective bands located between 490 nm and 580 nm, we used alternating SiO_2 and Ta_2O_5 layers. Metasurface structures were directly fabricated on the surface of dielectric mirrors, details are provided in Supplementary Information Fig.S1 and Note 3. For the metasurface-embedded DBR which reflective bands located between 560

nm and 710 nm, we used 1 pairs of alternating SiO_2 and Ta_2O_5 layers. The dye concentrations are 2 mM for Rhodamine 6G (R6G) used in paper was purchased from Sigma Aldrich (#83697), with an excitation wavelength of 530 nm. The spacer inside the F-P cavity is the glass beads with a diameter around 28, 33, 45 μm, so that the cavity length equals 28, 33, 45 μm.

4.3 Numerical simulation

Numerical simulations in Fig. 2, Fig. 6b, Fig. S9, Fig. S10, and Fig. S11 were performed with the commercial software CST Microwave Studio. To calculate the optical response for an array of nanostructures, the unit cell boundary condition is applied for both x- and y-directions. The incident electric field is expressed by $\vec{E}(z,t) = \hat{x}E_0 e^{-i(kz+\varphi)}$, where E_0 is the amplitude, k is the wavenumber, ϕ is the initial phase, and ω is the angular frequency. The time-dependent field distribution (stable condition after multiple times of meta-light-matter interactions) can be obtained by varying the initial phase ϕ.

5. Funding, acknowledgments, and disclosures

5.1 Funding

5.2 Acknowledgments

5.3 Disclosures
The authors declare no conflicts of interest

References

1.   B. Peng, Ş. K. Özdemir, S. Rotter, H. Yilmaz, M. Liertzer, F. Monifi, C. M. Bender, F. Nori, and L. Yang, "Loss-induced suppression and revival of lasing," Science **346**, 328-332 (2014).
2.   Z. Zhang, X. Qiao, B. Midya, K. Liu, J. Sun, T. Wu, W. Liu, R. Agarwal, J. M. Jornet, and S. Longhi, "Tunable topological charge vortex microlaser," Science **368**, 760-763 (2020).
3.   Z. Yuan, X. Tan, X. Gong, C. Gong, X. Cheng, S. Feng, X. Fan, and Y.-C. Chen, "Bioresponsive microlasers with tunable lasing wavelength," Nanoscale **13**, 1608-1615 (2021).
4.   Z. Yuan, Z. Wang, P. Guan, X. Wu, and Y. C. Chen, "Lasing-Encoded Microsensor Driven by Interfacial Cavity Resonance Energy Transfer," Adv. Opt. Mater. **8**, 1901596 (2020).

5.   S.-J. Tang, P. H. Dannenberg, A. C. Liapis, N. Martino, Y. Zhuo, Y.-F. Xiao, and S.-H. Yun, "Laser particles with omnidirectional emission for cell tracking," Light Sci. Appl. **10**, 1-11 (2021).

6.   C. Wang, C. Gong, Y. Zhang, Z. Qiao, Z. Yuan, Y. Gong, G.-E. Chang, W.-C. Tu, and Y.-C. Chen, "Programmable rainbow-colored optofluidic fiber laser encoded with topologically structured chiral droplets," ACS Nano **15**, 11126-11136 (2021).

7.   Z. Yuan, Y. Zhou, Z. Qiao, C. Eng Aik, W.-C. Tu, X. Wu, and Y.-C. Chen, "Stimulated Chiral Light–Matter Interactions in Biological Microlasers," ACS Nano **15**, 8965-8975 (2021).

8.   Z. Yuan, X. Cheng, Y. Zhou, X. Tan, X. Gong, H. Rivy, C. Gong, X. Fan, W.-J. Wang, and Y.-C. Chen, "Distinguishing Small Molecules in Microcavity with Molecular Laser Polarization," ACS Photonics **7**, 1908-1914 (2020).

9.   N. Hafi, M. Grunwald, L. S. Van Den Heuvel, T. Aspelmeier, J.-H. Chen, M. Zagrebelsky, O. M. Schütte, C. Steinem, M. Korte, and A. Munk, "Fluorescence nanoscopy by polarization modulation and polarization angle narrowing," Nat. Methods **11**, 579-584 (2014).

10.   K. Zhanghao, X. Chen, W. Liu, M. Li, Y. Liu, Y. Wang, S. Luo, X. Wang, C. Shan, and H. Xie, "Super-resolution imaging of fluorescent dipoles via polarized structured illumination microscopy," Nat. Commun. **10**, 1-10 (2019).

11.   M. Wang, M. Chen, K. Zhanghao, X. Zhang, Z. Jing, J. Gao, M. Q. Zhang, D. Jin, Z. Dai, and P. Xi, "Polarization-based super-resolution imaging of surface-enhanced Raman scattering nanoparticles with orientational information," Nanoscale **10**, 19757-19765 (2018).

12.   A. E. Siegman, *Lasers* (University Science Books, 1986).

13.   M. Wang, Y. Lin, J.-M. Yi, D.-Y. Li, J.-P. Liu, B. Cao, C.-H. Wang, J.-F. Wang, and K. Xu, "High-efficiency circularly polarized green light emission from GaN-based laser diodes integrated with GaN metasurface quarterwave plate," Appl. Phys. Lett. **119**, 241103 (2021).

14.   Y.-Y. Xie, P.-N. Ni, Q.-H. Wang, Q. Kan, G. Briere, P.-P. Chen, Z.-Z. Zhao, A. Delga, H.-R. Ren, and H.-D. Chen, "Metasurface-integrated vertical cavity surface-emitting lasers for programmable directional lasing emissions," Nat. Nanotechnol. **15**, 125-130 (2020).

15.   L. Xu, D. Chen, C. A. Curwen, M. Memarian, J. L. Reno, T. Itoh, and B. S. Williams, "Metasurface quantum-cascade laser with electrically switchable polarization," Optica **4**, 468-475 (2017).

16.   A. H. Dorrah, N. A. Rubin, A. Zaidi, M. Tamagnone, and F. Capasso, "Metasurface optics for on-demand polarization transformations along the optical path," Nat. Photonics **15**, 287-296 (2021).

17.   C. Huang, C. Zhang, S. Xiao, Y. Wang, Y. Fan, Y. Liu, N. Zhang, G. Qu, H. Ji, and J. Han, "Ultrafast control of vortex microlasers," Science **367**, 1018-1021 (2020).

18.   H. Sroor, Y.-W. Huang, B. Sephton, D. Naidoo, A. Vallés, V. Ginis, C.-W. Qiu, A. Ambrosio, F. Capasso, and A. Forbes, "High-purity orbital angular momentum states from a visible metasurface laser," Nat. Photonics (2020).

19.   P. C. Wu, W.-Y. Tsai, W. T. Chen, Y.-W. Huang, T.-Y. Chen, J.-W. Chen, C. Y. Liao, C. H. Chu, G. Sun, and D. P. Tsai, "Versatile polarization generation with an aluminum plasmonic metasurface," Nano Lett. **17**, 445-452 (2017).

20.   A. E. Minovich, A. E. Miroshnichenko, A. Y. Bykov, T. V. Murzina, D. N. Neshev, and Y. S. Kivshar, "Functional and nonlinear optical metasurfaces," Laser Photonics Rev. **9**, 195-213 (2015).

21.   A. Vaskin, R. Kolkowski, A. F. Koenderink, and I. Staude, "Light-emitting metasurfaces," Nanophotonics **8**, 1151-1198 (2019).

22.   A. M. Shaltout, J. Kim, A. Boltasseva, V. M. Shalaev, and A. V. Kildishev, "Ultrathin and multicolour optical cavities with embedded metasurfaces," Nat. Commun. **9**, 1-7 (2018).

23.   R. Ameling, and H. Giessen, "Microcavity plasmonics: strong coupling of photonic cavities and plasmons," Laser Photonics Rev. **7**, 141-169 (2013).

24.   T. D. Barrett, O. Barter, D. Stuart, B. Yuen, and A. Kuhn, "Polarization oscillations in birefringent emitter-cavity systems," Phys. Rev. Lett. **122**, 083602 (2019).

25.   X. Fan, and S.-H. Yun, "The potential of optofluidic biolasers," Nat. Methods **11**, 141-147 (2014).

26.   Y.-T. Lin, A. Hassanfiroozi, W.-R. Jiang, M.-Y. Liao, W.-J. Lee, and P. C. Wu, "Photoluminescence enhancement with all-dielectric coherent metasurfaces," Nanophotonics **11**, 2701-2709 (2022).

27.   Z. Wang, Y. Wang, G. Adamo, J. Teng, and H. Sun, "Induced optical chirality and circularly polarized emission from achiral CdSe/ZnS quantum dots via resonantly coupling with plasmonic chiral metasurfaces," Laser Photonics Rev. **13**, 1800276 (2019).

28.   H. Kogelnik, and T. Li, "Laser beams and resonators," Applied optics **5**, 1550-1567 (1966).

29.   K. Voronin, A. S. Taradin, M. V. Gorkunov, and D. G. Baranov, "Single-handedness chiral optical cavities," ACS Photonics **9**, 2652-2659 (2022).

30.   X. Fang, K. F. MacDonald, E. Plum, and N. I. Zheludev, "Coherent control of light-matter interactions in polarization standing waves," Sci. Rep. **6**, 1-7 (2016).